Export of nutrient rich Northern Component Water preceded early Oligocene Antarctic glaciation

Authors: Helen K. Coxall[1], Claire Huck[2,3], Matthew Huber[4,5], Caroline H. Lear[6], Alba Legarda-Lisarri[10], Matt O'Regan[1], Kasia K. Sliwinska[7,8], Tina van de Flierdt[2], Agatha M. de Boer[1], James C. Zachos[9] & Jan Backman[1]

Affiliations:
[1]Department of Geological Sciences, Stockholm University, SE-106 91 Stockholm, Sweden.
[2]Department of Earth Science and Engineering, Imperial College London, South Kensington Campus, London SW7 2AZ, UK.
[3]Ocean and Earth Science, National Oceanography Centre Southampton, University of Southampton, European Way, Southampton SO14 3ZH, UK.
[4]Department of Earth Sciences, University of New Hampshire, Durham, NH 03824, USA.
[5]Earth Systems Research Center, Institute for Earth, Ocean and Space Sciences, The University of New Hampshire, Durham NH, USA.
[6]School of Earth and Ocean Sciences, Cardiff University, Main Building, Park Place, Cardiff CF10 3AT, UK.
[7]Geological Survey of Denmark and Greenland, GEUS, Øster Voldgade 10, DK-1350, Copenhagen K, Denmark.
[8]NIOZ Royal Netherlands Institute for Sea Research, Department of Marine Organic Biogeochemistry, P.O. Box 59, 1790 AB Den Burg, Texel, The Netherlands.
[9]Earth & Planetary Sciences Department, University of California, Santa Cruz, CA 95064, USA.
[10]Department of Earth Sciences, University of Zaragoza, Pedro Cerbuna Street, 12, 50009 Zaragoza, Spain.

Onset of North Atlantic deep water formation is thought to have coincided with Antarctic ice sheet growth about 34 million years ago. However, this timing is debated, in part due to questions over the geochemical signature of ancient Northern Component Water formed in the deep North Atlantic. Here we present detailed geochemical records from North Atlantic sediment cores located close to sites of deep water formation. We find that prior to 36 million years ago, the northwestern Atlantic was stratified, with nutrient-rich, low salinity bottom waters. This restricted basin transitioned into a conduit for Northern Component Water that began flowing southwards approximately one million years before initial Antarctic glaciation. The probable trigger was tectonic adjustments in subarctic seas that enabled increased exchange across the Greenland-Scotland Ridge. Increasing surface

salinity and density strengthened Northern Component Water production. The late Eocene deep water mass differed in its carbon isotopic signature from modern as a result of leakage of fossil carbon from the Arctic Ocean. Export of this nutrient-laden water provided a transient pulse of CO_2 to the Earth system perhaps causing short-term warming, whereas the long-term effect of enhanced NCW formation was greater northward heat transport that cooled Antarctica.

Production of deep water in the North Atlantic Ocean plays a vital role in maintaining the global meridional overturning circulation (MOC)[1]. North Atlantic Deep Water (NADW), the lower branch of the Atlantic part of the MOC (AMOC), forms in the Labrador and Nordic Seas as surface waters cool and densify. The sinking is largely controlled by an interplay of (i) the stratification at convection sites, determined by the balance of warm salty water from low latitudes, cold freshwater from the Arctic Ocean, and local heat and freshwater fluxes, and (ii) wind-driven upwelling in the Southern Ocean, which returns deep water to the surface[2,3]. Both factors likely impacted the early Cenozoic MOC state, when Atlantic bathymetry and ocean gateways were different and global temperatures were warmer than today[4,5]. However, resolving their interplay at the onset of NADW production, referred to here as its palaeo pre-cursor Northern Component Water (NCW), is challenging because the early history of the AMOC remains poorly constrained.

Benthic foraminifera $\delta^{18}O$ and $\delta^{13}C$ records constrain development of global deep water circulation by giving insights into subsurface temperatures, salinity and nutrients[5]. A widely held view is that NCW began filling the Atlantic close to the Eocene-Oligocene greenhouse to icehouse climate transition (EOT), ~34 million years ago (Ma)[4,6-9], or earlier[10-13]. Others argue that emergence of significant NCW was delayed until the late Miocene[14]. Modeling studies diverge, suggesting either no NCW[15] during the EOT, strengthening/onset of bipolar deep water formation triggered by Drake Passage deepening[16-18], or an ocean state with robust NCW throughout[19]. Previous data studies that argue for a late Eocene onset of NCW production assume that early Cenozoic NCW was nutrient-poor with a high ('young') benthic $\delta^{13}C$ signature similar to modern well ventilated NADW[4,10,13,20]. Yet palaeo data from northerly regions suitable for characterizing NCW are lacking.

To fill this gap, we produced EOT benthic $\delta^{13}C$ and $\delta^{18}O$ records from four deep sea sites (>1000 m palaeodepth) in the high latitude North Atlantic (see Methods and Supplementary Information). Of these, Site 647 in the Southern Labrador Sea (SLS; 47°N, 34 Ma palaeolatitude, ~2000-3000 m palaeodepth), is the most northerly EOT sequence containing calcareous microfossils necessary for $\delta^{18}O$ and $\delta^{13}C$ analysis[21]. Additional data for portions of the late Eocene were generated from DSDP Sites 112 and 612, and IODP Site U1411 (Fig. 1). The latter two sites should record NCW export in the deep western boundary current (DWBC) (Fig. 1). The data are compared against an Atlantic isotope compilation incorporating 14 previously investigated sites (Fig. 2). Records of benthic foraminifera Mg/Ca, fish tooth εNd, and planktic foraminifera $\delta^{18}O$ and $\delta^{13}C$ from Site 647 and U1411 were also generated to provide constraints on bottom water temperature (BWT) and provenance, and water column structure (Methods). The results add unique perspectives on Atlantic end-member deep water properties and changes in circulation during the EOT.

High nutrient content of late Eocene Southern Labrador Sea deep waters

At Site 647 we recognize the typical pattern of $\delta^{18}O$ and $\delta^{13}C$ increase (>1.0‰ and ~0.5 to 1.0‰ respectively) between 34-33.5 Ma diagnostic of early Oligocene Antarctic glaciation, including the peak in $\delta^{18}O$ seen at other sites[22], here referred to as the Early Oligocene Glacial Maximum (EOGM) (Fig. 2). The first novel observation at Site 647 is that before ~35.8 Ma, $\delta^{13}C$ of SLS bottom water is on average 0.5-1 ‰ lower than all southerly sites. This is opposite to the modern AMOC state, where northern deep waters have the highest $\delta^{13}C$ due to sinking of well ventilated, nutrient poor surface waters[23]. The low $\delta^{13}C$ may reflect nutrient accumulation under stratified conditions analogous to the modern North Pacific, i.e. the end of the circulation path. This could imply a southern-sourced deep water filled the SLS during the late Eocene. However, Site 647 fish debris εNd, an isotopic tracer for the origin of deep water masses, bear the fingerprint of a northern hemisphere source (εNd = -11.4 to -9.4) throughout the studied interval (Fig. 3g). Consequently, we instead argue the low benthic $\delta^{13}C$ reflects local bottom water sourced from surface waters with a high nutrient concentration, within the narrow, restricted North Atlantic basinal deep water circulation. A probable nutrient source is 'fossil' carbon leaking in from the Arctic Ocean and subarctic seas (Greenland and Norwegian Seas), which had high nutrient stocks during the Eocene because of their semi-isolation, heavily vegetated margins[24], and high riverine inflow[25-27].

We identify three circulation regimes based on our new Eocene-Oligocene proxy records and comparisons with published data (Figs. 2 and 3). Focusing first on $\delta^{13}C$ (Fig. 2), under Regime 1 (>35.8 Ma), SLS bottom waters were isolated from the rest of the Atlantic and a distinct NCW with low $\delta^{13}C$ bathed Site 647. After ~35.8 Ma an approximately 1.5-2 million year-long (~35.8 to ~ 33.8 Ma) negative $\delta^{13}C$ excursion (0.5-1‰ $\delta^{13}C$ decrease) is seen to varying degrees at Sites 612, U1411 and 647, as well as some other Atlantic sites (1053, 1090, 366). Offsets in this excursion's timing between sites are likely caused by age model differences. The phase encompassing the onset and peak of the excursion is Regime 2. Importantly, the $\delta^{13}C$ excursions are largest (maximum 1‰) at Sites 612 and U1411 sitting in the DWBC (Fig. 1). While noted previously[28], the wider significance of this $\delta^{13}C$ excursion has not been fully explored. The observation that Sites 612 and U1411, directly down stream of Site 647, gain benthic $\delta^{13}C$ signals close to the SLS end-member suggests the signal was propagated from the north. Thus it records southward export of Arctic imprinted, nutrient-rich NCW. The increase in Atlantic benthic $\delta^{13}C$ towards the end of Regime 2 indicates that either the pulse of NCW ended, or sufficiently ventilated surface water with higher $\delta^{13}C$ was imported to convection sites. Regime 3, described below, represents the phase where a more mature form of NCW existed.

Northern deep water cooling, salinification and destratification

A second prominent feature is the pattern of SLS benthic $\delta^{18}O$. The majority of pre-Oligocene $\delta^{18}O$ data south of Site 647 range between 0.4-1.2‰ (Fig. 2). Strikingly, in the SLS during Regime 1, benthic $\delta^{18}O$ is 1-3‰ lower than the ensemble. The primary controls on benthic $\delta^{18}O$ are BWT and the $\delta^{18}O$ composition of seawater, the latter reflecting global glacial ice volume and local salinity. Assuming minimal ice before 34 Ma, the relatively low $\delta^{18}O$ in SLS benthos indicates a considerably warmer or fresher water mass bathing the seafloor compared to southern stations. Benthic $\delta^{18}O$ from Sites 647 and 112 increased gradually from 36.0 to 35.4 Ma, then again from ~34.6-34.4 Ma, and had converged close to the dominant Atlantic trend by ~34.3 Ma, i.e. coincident with or just lagging the Atlantic-wide $\delta^{13}C$ minimum. Diagenetic alteration of Site 647 benthic fossils[29] is ruled out due to (i) the excellent fossil calcite preservation[21] (Supplementary Information), and (ii) the similarity of our new planktic $\delta^{18}O$ values from Sites

647 and U1411 (Fig. 3). Moreover, a similar pattern of decreasing benthic $\delta^{18}O$ is seen in a North Sea record[30], although at shallower depths (~500m).

Mg/Ca BWT help deconvolve temperature and salinity influences on $\delta^{18}O$ (Methods and Supplementary Information). Across the EOT, Site 647 Mg/Ca data suggest BWT cooling of ~1˚C combined with a ~0.6‰ increase in $\delta^{18}O_{sw}$, in agreement with previous studies[31] (Fig. 3a). From this, we estimate gradual bottom water cooling in the SLS of ~3-4°C between 37.5 Ma to 35 Ma, which is similar to observed northern high latitude sea surface coolings[32]. Substituting the Mg/Ca BWTs into a $\delta^{18}O$ palaeotemperature equation (Methods) yields ice-free $\delta^{18}O_{sw}$ estimates of between -3 to -4 ‰ SMOW during this interval. Based on these $\delta^{18}O_{sw}$ constraints, we estimate late Eocene SLS bottom salinities using relevant modern $\delta^{18}O_{sw}$-sea surface salinity (SSS) relationships[33] (Fig. 3c).

Applying a modern SSS-$\delta^{18}O_{sw}$ relationship from eastern Greenland, today a conduit for low salinity (32 PSU) Arctic outflow, implies Site 647 bottom water salinity of 30-32 PSU before 36 Ma, increasing by 2-3 PSU from 36 to 34 Ma. The salinity change is similar when a Laptev Sea (today fed by large Siberian rivers) $\delta^{18}O_{sw}$-salinity regression is applied. While SSS-$\delta^{18}O_{sw}$ relationships are spatially widely variable, and modern relationships are only loose analogues for the Eocene, our inferred values are compatible with modern temperature-salinity fields. Therefore, we suggest that (i) before 36 Ma SLS bottom waters were relatively fresh, and (ii) SLS bottom salinity increased from Regime 1 to 2. This conclusion does not change even if samples older than 35 Ma are biased to higher Mg (Supplementary Information) since the salinity signal is embedded in the benthic $\delta^{18}O$, which is independent of Mg/Ca. This interpretation is consistent with that for pre-formed nutrients—they are both likely derived from the Arctic Ocean. Proxies and models agree that the Arctic had a thick freshwater cap during the Palaeogene as a consequence of a strong hydrological system and high fluvial inputs under greenhouse forcing, combined with restricted salt input[26,33-35]. With no Pacific Ocean outlet at this time, major surface discharge occurred through the Nordic Seas[34,36].

Site 647 planktic foraminifera $\delta^{18}O$ and $\delta^{13}C$ add information on the upper water column. $\delta^{18}O$ of mixed layer (surface) species is 1-2 ‰ lower than deep-dwellers (subthermocline), consistent with a stratified upper ocean and calcification of mixed-layer dwellers high in the water column or during the warmest season (Fig. 3b). During Regime 1, and before 34.5 Ma, $\delta^{18}O$ of the deep-dwelling planktic species is indistinguishable from benthic foraminifera, reflecting influence of relatively fresh deep water at sub-thermocline levels in the SLS. Site 647 planktic data are sparse before 35 Ma due to low foraminiferal abundance and coring gaps. However, after 34.5 Ma, deep-dwelling planktic and benthic $\delta^{18}O$ records separate coincident with the appearance of deep water with temperature and salinity properties similar to typical Atlantic values. Additionally, a progressive collapse in the planktic – benthic $\delta^{13}C$ gradient (Fig. 3d, e) is documented that captures the SLS water column transitioning from being well-stratified with large vertical $\delta^{13}C$ differences (1-1.5 ‰) during Regime 1, to a state with a smaller $\delta^{13}C$ gradient (0.5‰) comparable to better-mixed modern North Atlantic convection sites[23] by ~34.3 Ma. Both observations are consistent with increasing NCW volume. An abrupt shift in Site 647 benthic assemblages at 34.3 Ma from agglutinated species tolerant of carbonate-poor, nutrient-rich environments, to calcareous species suited to stronger current flow[37] coincident with other changes (Fig. 3f), provides further evidence for increased convection. Circulation Regime 3 begins at 34.3 Ma, when a saltier, denser form of NCW with higher $\delta^{13}C$ is exported through the SLS.

Deep water sources and sinking

Our Site 647 fish debris εNd data behave as a conservative tracer of northern sourced deep water (see Supplementary Information) and can be compared to published ocean references[38,39] to identify probable NCW source regions (Fig. 3g). While we do not reconstruct Nd directly for Regime 1, our sample from 39 Ma is similar to the rest of the record, implying no systematic change in εNd and thus bottom water provenance as NCW evolved. The comparison suggests that the Southern Ocean, which has the highest end-member εNd signature in our compilation, was not the source of bottom waters at Site 647. Moreover we do not find evidence for the prominent EOT shift to high εNd values found in Southern Ocean records[40]. Previous studies have suggested that prior to deepening of the Greenland Scotland Ridge (GSR) NCW was sourced from the Labrador Sea[10,13]. Modern Labrador Sea deep water, however, has characteristically low εNd (~ -14), reflecting erosional inputs from the cratonic hinterland[41]. In contrast, Site 647 Nd is significantly more radiogenic (εNd = -11.4 to -9.4), and a closer match to the range of values measured in Nordic sea overflows (εNd = ~ -12.0 to -8.4)[41,42] and proximal Arctic Ocean basins above 500 m (εNd = -11.7 to -8.8)[43]. A Palaeogene presence of Tethys-sourced deep water at Site 647 is another possibility, since the Tethyian εNd signature (εNd = -10.0 to -9.3 [44,45]) is indistinguishable from that of North Atlantic water masses. However, palaeogeographic reconstructions suggest that water mass exchange between European Tethys and Nordic Seas was limited during the middle to late Eocene[25,46] making this unlikely.

The only connections between the Arctic Ocean and Nordic Seas during the Palaeogene were shallow[27,46,47]. Transfer of freshened, nutrient-rich waters from the Arctic would have occurred via a proto Greenland Current. Similarity between the North Sea (Kysing-4, borehole) and Site 647 benthic $\delta^{18}O$, as well as independent evidence for low salinities in the Nordic Seas[34,48], is consistent with this picture. Transport from the subarctic seas to the Atlantic Ocean was also shallow, and sinking of Arctic imprinted NCW, must have taken place south of the GSR until it subsided. With sufficient cooling in the subarctic seas, the density contrast of brackish Arctic waters with warmer saltier North Atlantic surface waters permitted sinking, resulting in the distinct bottom water recorded at Site 647.

Importantly, before ~ 36 Ma, Arctic imprinted NCW deep water formation was minimal, implying regular stratification and stagnation in the SLS. This is consistent with the considerable noise in $\delta^{13}C$ and $\delta^{18}O$ during Regime 1. How this deep water remained isolated in the SLS at depths of around 2000 m under Regime 1 remains uncertain. One possibility is that production and export rates of local deep waters in the North Atlantic were high compared to the influx of southern-sourced deep waters, and subsequently increased further as the cooler, saltier NCW started being produced. Alternatively, bathymetric highs associated with the now extinct Labrador Sea spreading ridges and the West Thulean igneous province to the south, may have isolated SLS subsurface waters from the overall Atlantic during the early Palaeogene[7]. In this case, cessation of Labrador Sea spreading close to the EOT was likely important, allowing ridges to subside and enabling enhanced deep water export.

We illustrate the isotopic evidence and sequence of EOT oceanic changes using natural neighbour re-gridding (Methods) of compiled isotopic data to produce south–north Atlantic depth transects during time windows centered on circulation Regimes 1-3 (Fig. 4, see Supplementary Information for data sources, additional transects and maps). Before ~36 Ma (Regime 1), a strong isotopic $\delta^{18}O$ and $\delta^{13}C$ depletion effects water masses down to ~2000 m above 40°N (Fig. 4a and b), corresponding to small amounts of low salinity, high nutrient Arctic imprinted NCW in the SLS. The rest of the Atlantic is filled with deep waters with more homogenous $\delta^{18}O$ sourced from southerly and possibly low latitude regions[10,13]. Increasing subarctic $\delta^{18}O$, reflecting progressive salinification and densification of Nordic surface waters, is accompanied by a 0.5 – 1.0 Myr pulse of NCW export during Regime 2 (Figs. 4 c to h). By 33.3-34.3 Ma the ‘fresh’ SLS deep water signal no longer exists, bottom water $\delta^{13}C$ increased, the acute phase of low $\delta^{13}C$ export is over, and a better-ventilated NCW is exported (Regime 3). Importantly, the initial pulse of NCW export under Regime 2 is recorded by decreasing $\delta^{13}C$ signals in deep waters down stream of the SLS. The presence of late Eocene NCW in the Atlantic has not been identified in previous $\delta^{13}C$ records[10,13,20] because NCW was assumed to have high $\delta^{13}C$ signature similar to modern NADW.

Causes and consequences of Northern Component Water export

Deepening of the GSR in the late Eocene, for which there is geological evidence[4,34], would have increased Nordic overflows, thus strengthening NCW production. Modelling suggests sill deepening to 50 m would initiate a threshold switch from lagoonal to estuarine circulation, salinifying the Nordic Seas sufficiently to intensify northern deep water production[34]. While this idea is consistent with our findings, the bathymetric history of the GSR is currently too crude to accurately date such a change. Moreover, we propose that contemporaneous restrictions to the Arctic-Nordic Sea exchange also played a role. Geological evidence suggests that the Barents Sea-Arctic passageway shoaled in the latest Eocene[46,47] and that relative sea-level variations in the Arctic were decoupled from global trends from the late Eocene to early Miocene[49]. This palaeogeographic Arctic isolation enhanced salinification in the Nordic Seas as brackish Arctic outflows were gradually cut off.

Changes in NCW production had varied and competing effects. Its onset presumably impacted poleward heat transport in both hemispheres[17,18]. Initial export of nutrient rich Arctic imprinted NCW may have generated a short-lived pulse of CO_2, on the order of 100-200 ppm, which is consistent with proxy compilations showing a temporary reversal in the falling CO_2 trend between ~34 to ~35 Ma[50]. On the other hand, strengthening of NCW production, and enhanced northward ocean heat transport, could have played a role in longer-term CO_2 drawdown due to an accompanying increase in rainfall over land and associated CO_2–weathering feedbacks[16]. The circulation change timing, 1-2 million years prior to Antarctic glaciation, reinforces the idea that onset of NCW played a role in preconditioning the late Eocene Earth system for the greenhouse to icehouse transition.

Methods

Methods, including statements of data availability and any associated accession codes and references, are available in the online version of this paper.

References

1 Broecker, W. S. Paleocean circulation during the last deglaciation: A bipolar seesaw? *Paleoceanography* **13**, 119-121 (1998).

2 de Boer, A. M., Toggweiler, J. R. & Sigman, D. M. Atlantic dominance of the meridional overturning circulation. *J. of Phys. Oceanog.* **38**, 435-450 (2008).

3 Toggweiler, R. & Samuels, B. Effect of Drake Passage on the global thermohaline circulation. *Deep Sea Res., Pt. 1* **42**, 477-500 (1995).

4 Abelson, M. & Erez, J. The onset of modern-like Atlantic meridional overturning circulation at the Eocene-Oligocene transition: Evidence, causes, and possible implications for global cooling. *Geochem., Geophys., Geosystems* **18**, 2177-2199 (2017).

5 Cramer, B. S., Toggweiler, J. R. T., Wright, J. D., Katz, M. E. & Miller, G. H. Ocean overturning since the Late Cretaceous: Inferences from a new benthic foraminiferal isotope compilation. *Paleoceanography* **24**, PA4216 (2009).

6 Davies, R., Cartwright, J., Pike, J. & Line, C. Early Oligocene initiation of North Atlantic Deep Water formation. *Nature* **410**, 917-920 (2001).

7 Egloff, J. & Johnson, G. L. Morphology and structure of the Southern Labrador Sea. *Canadian J. of Earth Sci.* **12**, 2111-2133 (1975).

8 Miller, K. G. & Tucholke, B. E. in *Structure and development of the Greenland-Scotland Ridge* (eds M.H.P. Bott, J. Thiede, S. Saxov, & M. Talwani) 549-589 (Plenum Press, 1983).

9 Via, R. K. & Thomas, D. J. Evolution of Atlantic thermohaline circulation: Early Oligocene onset of deep-water production in the North Atlantic. *Geology* **34**, 441-444 (2006).

10 Borrelli, C., Cramer, B. S. & Katz, M. E. Bipolar Atlantic deepwater circulation in the middle-late Eocene: effects of Southern Ocean gateway openings. *Paleoceanography* **29**, 308-327 (2014).

11 Boyle, P. R. *et al.* Cenozoic North Atlantic deep circulation history recorded in contourite drifts, offshore Newfoundland, Canada. *Marine Geology* **385**, 185-203 (2017).

12 Hohbein, M. W., Sexton, P. F. & Cartwright, J. A. Onset of North Atlantic Deep Water production coincident with inception of the Cenozoic global cooling trend. *Geology* **40**, 255-258 (2012).

13 Langton, S. J., Rabideaux, N. M., Borrelli, C. & Katz, M. E. Southeastern Atlantic deep-water evolution during the late-middle Eocene to earliest Oligocene (Ocean Drilling Program Site 1263 and Deep Sea Drilling Project Site 366). *Geosphere* **12**, 1032-1047 (2016).

14 Wright, J. D. & Miller, K. G. Control of North Atlantic Deep Water circulation by the Greenland-Scotland Ridge. *Paleoceanography* **11**, 157-170 (1996).

15 Sijp, W. P., England, M. H. & Huber, M. Effect of the deepening of the Tasman Gateway on the global ocean. *Paleoceanography* **26**, PA4207 (2011).

16 Elsworth, G., Galbraith, E., Halverson, G. & Yang, S. Enhanced weathering and CO2 drawdown caused by latest Eocene strengthening of the Atlantic meridional overturning circulation. *Nat. Geosci.* **10**, 213-216 (2017).

17 Tigchelaar, M., von der Heydt, A. S. & Dijkstra, H. A. A new mechanism for the two-step δ^{18}O signal at the Eocene-Oligocene boundary. *Clim. Past* **7**, 235-247 (2010).

18 Zhang, Z. *et al.* Tropical seaways played a more important role than high latitude seaways in Cenozoic cooling. *Clim. Past* **7**, 801-813 (2011).

19 Huber, M. & Sloan, L. C. Heat transport, deep waters, and thermal gradients: Coupled simulation of an Eocene greenhouse climate. *Geo. Res. Lett.* **28**, 3481-3484 (2001).

20 Pusz, A. E., Thunell, R. C. & Miller, K. G. Deep water temperature, carbonate ion, and ice volume changes across the Eocene-Oligocene climate transition. *Paleoceanography* **26**, PA2205 (2011).

21 Firth, J. V., Eldrett, J. S., Harding, I. C., Coxall, H. K. & Wade, B. Integrated biomagnetochronology for the Palaeogene of ODP Hole 647A: Implications for correlating palaeoceanographic events from high to low latitudes. *Geol. Soc. Spec. Pub.* **373**, 29-78 (2013).

22 Coxall, H. K. & Wilson, P. A. Early Oligocene glaciation and productivity in the eastern equatorial Pacific; insights into global carbon cycling. *Paleoceanography* **26**, PA2221 (2011).

23 Kroopnick, P. The distribution of ^{13}C of $\sum CO_2$ in the world oceans. *Deep Sea Res.* **32**, 57-84 (1985).

24 Golovneva, L. B. Early Palaeogene floras of Spitsbergen and North Atlantic floristic exchange. *Acta Universitatis Carolinae, Geologica* **44**, 39-50 (2000).

25 Akhmetiev, M. A. & Beniamovski, V. N. Paleogene floral assemblages around epicontinental seas and straits in Northern Central Eurasia: proxies for climatic and paleogeographic evolution. *Geologica Acta* **7**, 297-309 (2009).

26 Gleason, J. D. *et al.* Early to middle Eocene history of the Arctic Ocean from Nd-Sr isotopes in fossil fish debris, Lomonosov Ridge. *Paleoceanography.* **24,** PA2215 (2009).

27 O'Regan, A. M., Williams, C. J., Frey, K. E. & Jakobsson, M. A Synthesis of the long-term paleoclimatic evolution of the Arctic. *Oceanography, The changing Arctic Ocean, Special Issue on the International Polar Year (2007–2009)* **24**, 66-80 (2011).

28 Pusz, A. E. *et al.* in *Special Paper of the Geol. Soc. of America*. **452,** 83-95 (2009).

29 Arthur, M. A. *et al.* in *Proceedings of the Ocean Drilling Program, Scientific Results* Vol. **105** (eds S.P. Srivastava, M.A. Arthur, B. Clement et al.) 111-135 (Ocean Drilling Program, 1989).

30 Nielsen, S. B. *et al.* The evolution of western Scandinavian topography: A review of Neogene uplift versus the ICE (isostasy–climate–erosion) hypothesis. *J. Geodynam.* **47**, 72-95 (2009).

31 Lear, C. H., Bailey, T. R., Pearson, P. N. P., Coxall, H. K. & Rosenthal, Y. Cooling and ice growth across the Eocene-Oligocene transition. *Geology* **36**, 251-254 (2008).

32 Liu, L. *et al.* Global cooling during the Eocene-Oligocene climate transition. *Science* **323**, 1187-1190 (2009).

33 Waddell, L. M. & Moore, T. C. Salinity of the Eocene Arctic Ocean from oxygen isotope analysis of fish bone carbonate. *Paleoceanography*, PA1S12 (2008).

34 Stärz, M., Jokat, W., Knorr, G. & Lohmann, G. Threshold in North Atlantic-Arctic Ocean circulation controlled by the subsidence of the Greenland-Scotland Ridge. *Nat. Comm.* **8**, 15681, doi:10.1038/ncomms15681 (2017).

35 Roberts, C. D., LeGrande, A. N. & Tripati, A. K. Climate sensitivity to Arctic seaway restriction during the early Paleogene. *Earth Planet. Sci. Lett.* **286**, 576-585 (2009).

36 Brinkhuis, H. *et al.* Episodic fresh surface waters in the Eocene Arctic Ocean. *Nature* **441**, 606-609 (2006).

37 Kaminski, M. & Ortiz, S. The Eocene-Oligocene turnover of deep-water agglutinated foraminifera at ODP Site 647, Southern Labrador Sea (North Atlantic). *Micropaleontology* **60**, 53-66 (2014).

38 Burton, K. W., Ling, H. F. & O'Nions, R. K. Closure of the Central American isthmus and its effect on deep-water formation in the North Atlantic. *Nature* **386**, 382-385 (1997).

39 O'Nions, R. K., Frank, M., von Blanckenburg, F. & Ling, H. F. Secular variation of Nd and Pb isotopes in ferromanganese crusts from the Atlantic, Indian and Pacific Oceans. *Earth Planet. Lett.* **155**, 15-28 (1998).

40 Scher, H. D. & Martin, E. E. Timing and climatic consequences of the opening of Drake Passage. *Science* **312**, 428-430 (2006).

41 Lambelet, M. *et al.* Neodymium isotopic composition and concentration in the western North Atlantic Ocean: Results from the GEOTRACES GA02 section. *Geochem. Cosmochim. Acta* **177**, 1-29 (2016).

42 Lacan, F. & Jeandel, C. Acquisition of the neodymium isotopic composition of the North Atlantic Deep Water. *Geochem., Geophys., Geosystems.* **6** (2005).

43 Porcelli, D. *et al.* The distribution of neodymium isotopes in Arctic Ocean basins. *Geochim. Cosmochim. Acta* **73**, 2645-2659 (2009).

44 Grandjean, P., Cappetta, H., Michard, A. & Albarede, F. The assessment of REE patterns and 143Nd/144Nd Nd ratios in fish remains. *Earth Planet. Sci. Lett.* **84**, 181-196 (1987).

45 Stille, P. & Fischer, H. Secular variation in the isotopic composition of Nd in Tethys seawater. *Geochim. Cosmochim. Acta* **54**, 3139-3145 (1990).

46 Kharin, G. S. & Lukashina, N. P. Paleogeography of the Norwegian-Greenland and northwestern European Sea basins in the Paleogene. *Oceanology* **50**, 226-239 (2010).

47 Musatov, E. E. & Pogrebitskij, Y. E. Late Mesozoic-Cenozoic evolution of the Barents Sea and Kara Sea continental margins. *Polarforschung* **68**, 283-290 (2000).

48 Andreasson, F. P., Schmitz, B. & Spiegler, D. in *Proceedings of the Ocean Drilling Program, Scientific Results.* Vol. **151** (eds J. Thiede *et al.*) 583-591 (Ocean Drilling Program, 1996).

49 Hegewald, A. & Jokat, W. Relative sea level variations in the Chukchi region - Arctic Ocean - since the late Eocene. *Geophys. Res. Lett.* **40**, 2013 (2013).

50 Anagnostou, E. *et al.* Changing atmospheric CO_2 concentration was the primary driver of early Cenozoic climate. *Nature* **533**, 380-384 (2016).

Corresponding Author Correspondence and requests for materials should be addressed to Helen Coxall (helen.coxall@geo.su.se).

Acknowledgements Samples were provided by the International Ocean Discovery Program (IODP), which includes the predecessors the Deep Sea Drilling Project and Ocean Drilling Program. We thank Julia Becker and Megan Spencer for technical assistance with the stable isotopes and Hedvig Öste and Emelie Axelsson for preparing the core samples. HKC was supported by a Royal Society Research Fellowship, Swedish Funding agency (VR) no. DNR 2008-2859 and the Bolin Centre for Climate Research, and TF by NERC Grants NE/I006257/1 and NE/L004607/1. KS acknowledges financial support from the Danish Council for Independent Research/Natural Sciences (DFF/FNU; Grant 11-107497).

Author Contributions HKC and JB conceived the project. HKC directed the research, generated the stable isotope data for Sites 112, 647 and U1411, compiled the proxy records and led writing of the paper. AL produced the new Site 612 data and age model. CHL conducted the trace metal analysis. CH produced and interpreted the Nd data with the help of TF. MO produced the palaeogeographic map for Figure 1 and conducted the subsidence modeling. KS helped produce the Site 647 age model. MH helped with the interpretative framework and produced the interpolated Atlantic depth isotopic transects and maps. JZ and AdB helped interpret the data. All authors contributed to writing the manuscript.

Additional information

Supplementary information is available in the online version of this paper. The data can be obtained from the 'Bolin Centre for Climate Research' database: http://bolin.su.se/data/Coxall-2018. Reprints and permissions information is available online at www.nature.com/reprints.

Competing financial interests

The authors declare no competing financial interests.

Figure captions

Figure 1. Site locations of sections included in this study. Stars identify the new data sets presented here. Map annotations: Red line = Mid Ocean Ridge 34 Ma; white line = position of 56 Ma isochron; black line = continent-ocean crust boundary. See Methods Section for details of the palaeogeographic framework and inset map. LS = Labrador Sea, NGS = Norwegian

Greenland Sea; T = Tethys Ocean; GSR = Greenland Scotland Ridge. Inset panel shows the path of major deep (blue) and surface currents today: Denmark Strait Overflow Water (DSOW); Iceland-Scotland Overflow Water (ISOW); Labrador Sea Water (LSW); North Atlantic Current (NAC) and the Deep Western Boundary Current (DWBC).

Figures 2. New and published Atlantic benthic $\delta^{18}O$ and $\delta^{13}C$ (*Cibs*. adjusted). The EOT (fine dashed horizontal lines) and the EOGM event are identified by the step-increase and maximum in $\delta^{18}O$ in the earliest Oligocene respectively. Trend lines represent smoothed curve fits that incorporate a geometric weighting. Regimes 1-3, separated by blue long-dash lines, are phases of ocean circulation defined here based on proxy data. Pale aqua shading represents transition phases. Vertical black arrows identify time windows gridded in Fig. 4. See Supplementary Information for data sources, age modeling and an expanded figure with additional data.

Figure 3. Sites 647 and U1411 multiproxy data. a) Mg/Ca BWT; paler blue symbols = maximum BWTs due to potential Fe contamination (Supplementary information). b), d): planktic and benthic $\delta^{18}O$ and $\delta^{13}C$ (black symbols=equatorial Pacific EOT chemostratigraphic reference[22], open symbols =U1411). c) Estimated Site 647 bottom salinity based on modern $\delta^{18}O_{sw}$- relationships; (LS) Laptev Sea, (EG) Eastern Greenland. Error envelopes are based on 2STD of the Mg/Ca BWT. e) =Site 647 planktic-benthic $\delta^{13}C$ difference and modern gradients[23]. f) Site 647 agglutinated benthic foraminifera[37]. g) Site 647 fish tooth Nd and EOT ocean signatures, including Artic ranges (error bars = 2σ standard reproducibility). Annotations as in Fig. 2.

Figure 4. Depth-latitude compilation of Atlantic benthic $\delta^{13}C$ and $\delta^{18}O$ during the late Eocene to early Oligocene constructed using natural neighbor interpolation. Data are plotted at their 34 Ma positions (dots indicate core palaeopositions). The five time slices illustrate the transition through the three circulation regimes identified here (R1, R2 and R3; see Fig. 2). See Supplementary information for data sources and a more extensive set of gridded time slices and late Eocene maps.

METHODS

Palaeogeographic plate reconstructions and modern Atlantic Ocean circulation inset

Palaeogeographic plate reconstructions used in production of main text Figure 1 were performed using G-plates, with coastlines adapted from E-O reconstructions (34 Ma) of Ron Blakey, Colorado Plateau Geosystems, Arizona USA. The inset figure showing modern North Atlantic surface and deep current paths is based on the schematics of ref-[51].

Age framework

Site 647 age control is based on biomagnetostratigraphy[21], adjusted here using Site 647 $\delta^{18}O$ chemostratigraphy (See Supplementary information for further details for Site 647 and the other sites). Site 112 ages are estimated from biostratigraphy[52]. Site U1411 ages are based on IODP Exp. 342 shipboard magnetostratigraphy[53]. The Site 612 age model is based on the biostratigraphy of ref-[54]. In all cases, datum events are calibrated or rescaled using linear interpolation to the chronology of ref-[55] to permit comparison with the Atlantic benthic isotope stack (after refs-[5,56,57]), much of which exists on this common time scale.

Stable isotopes

Planktic and benthic foraminifera are present throughout the EOT interval of Site 647, 112 and U1411, although heavily diluted by terrestrial clay. Planktic and benthic foraminifera are somewhat more common at Site 612. Tests are exceptionally well preserved at all sites throughout the studied intervals (see Supplementary Information for further details).

Foraminiferal $\delta^{18}O$ and $\delta^{13}C$ for Sites 647 and 112, was derived from the benthic foraminifera taxa *Oridorsalis umbonatus* (shallow infaunal) and *Cibicidoides* spp. (epifaunal), where available, both shown to be a reliable deep-sea tracer in previous studies[22,58] (see Supplementary Information). Site U1411 measurements are on *Cibicidoides* spp. and the new Site 612 measurements on *Hanzawaia ammophila*. Sites 647 and U1411 planktic foraminiferal analyses were made on *Turborotalia ampliapertura* and *Catapsydrax unicavus*, representing surface mixed layer and thermocline/subthermocline habitats respectively[59]. Site 647 stable isotope analysis was performed at Cardiff University using a ThermoFinnigan MAT252 mass spectrometer equipped with an automated KIEL III carbonate preparation unit. Additional samples were run at the National Oceanographic Centre, Southampton University, using a Europa Geo 20–20 mass spectrometer equipped with a CAPS automatic carbonate preparation system. Standard external analytical precision quoted at Cardiff was better than 0.05‰ for $\delta^{18}O$ and 0.03‰ for $\delta^{13}C$, and ±0.08‰ for $\delta^{18}O$ and $\delta^{13}C$ at Southampton. Site 612 analyses were measured at the Department of Geological Sciences, Stockholm University on a ThermoFinnigan MAT 252 IRMS coupled with a Finnigan Gasbench II device. Standard external analytical precision, based on replicate analysis of in-house standards calibrated to international standards (NBS19, IAEA-CO-1 and IAEA-CO-8), was better than 0.07‰ for $\delta^{13}C$ and 0.15‰ for $\delta^{18}O$. All results are reported relative to the VPDB standard. Our Site 647 *O. umbonatus* data have been adjusted to *Cibicidoides* values (believed to be close to ambient seawater) by subtracting -0.28‰ for the $\delta^{18}O$ following ref-[60], and by addition of 1.4‰ to the $\delta^{13}C$, following ref-[61] (consistent with a species comparison study in a restricted basin in the western North Pacific which closely matches our few Site 647 *Cibicidoides-Oridorsalis umbontatus* $\delta^{13}C$ pairs). The different species are differentiated in Figs. 2 and 3 by dark red (*O. umbontatus*) and bright red (*Cibicidoides* spp.) symbols. For Site 612 the following adjustments (after ref-[60]) were used when integrating the new *H. ammophila* data: ($\delta^{18}O_{H.\ ammophila}$ - 0.16)/0.62 = $\delta^{18}O_{Cibicidoides,}$ and $\delta^{13}C_{H.\ ammophila}$ + 0.08 = $\delta^{13}C_{Cibicidoides,}$ The planktic-benthic $\delta^{13}C$ gradient ($\Delta\delta^{13}C$) was generated by resampling the planktic and benthic foraminifera $\delta^{13}C$ curves to provide paired samples. Our new $\delta^{18}O$ and $\delta^{13}C$ are compared with 21 other Atlantic data sets that build on the compilations of refs-[5,57]. The new data produced in this study are presented in Supplementary Data file S1). See Supplementary Table S1 for the full list of sites meta data and sources used in our Atlantic compilation.

Trace metal analysis and Mg/Ca foraminiferal bottom water palaeothermometry

Trace metal content (Mg/Ca, Mn/Ca, Fe/Ca) was analyzed on Site 647 *O. umbonatus*. Prior to analysis, benthic foraminifera samples were cleaned following the protocol of refs-[62,63] leaving out the reducing step due to the scarcity of material but including contaminant removal under binocular microscope following the oxidative step[64]. Samples were subjected to one weak acid leach prior to dissolution and dilution. Analysis was carried out at Cardiff University on a Thermo Element XR ICP-MS against standards with equivalent Ca concentration. Multi-element standards were made in-house from single element standards supplied by Greyhound Chromatography and Allied Chemicals. Analytical precisions determined from separate consistency standards over the course of a year are 0.5% for Mg/Ca, and 2% for Mn/Ca and Fe/Ca (rsd). Mg/Ca paleo- bottom water temperatures (BWT) were calculated using the exponential calibration of ref-[58] (See Supplementary Information and Supplementary Data file S2).

Our *O. umbonatus* Mg/Ca record is noisy and high Mg/Ca ratios are often associated with high Fe/Ca (correlation coefficient $r^2 = 0.4$) (Supplementary Data file S2). By excluding the samples with Fe/Ca >> 900 µmol/mol, r^2 was reduced to 0.18. The subset of data, with lower Fe/Ca, largely the upper portion of the core in samples younger than 34.5 Ma (Supplementary Table S4), may be regarded as most reliable. However, despite the higher Fe/Ca in the older samples, we believe the Mg/Ca data from the lower part of the core are not entirely flawed since the Fe/Ca vs Mg/Ca r^2 value based on the full sample set is still relatively low and there is Mg/Ca overlap of higher and lower Fe/Ca Mg/Ca around the EOT (Main Figure 3A, paler blue symbols). Thus, the older Mg/Ca should provide realistic palaeo-bottom water temperatures (within the uncertainties of the method), and are thus included in the down core record to provide ballpark BWTs and allow salinity reconstructions in the initial part of the late Eocene.

Bottom Water Salinity reconstruction

The pattern of progressive benthic $\delta^{18}O$ increase and maximum 4°C BWT cooling between 37.5-35.5 Ma implies that sea water $\delta^{18}O$ ($\delta^{18}O_{sw}$) was changing over this period. To explore this further bottom water palaeosalinity was reconstructed based on modern sea surface salinity (SSS) - $\delta^{18}O$ relationships. This was performed in two steps. First, $\delta^{18}O_{sw}$ values were calculated by substituting the Site 647 Mg/Ca BWTs into the $\delta^{18}O$-benthic foraminifera palaeotemperature equation of ref-[65]. Due to the noise in our estimated benthic bottom water temperatures we used broad 'BWT brackets', based on mean BWT values for three intervals (Supplementary Table S5).

Second, bottom water palaeosalinity was reconstructed based on the modern surface salinity $\delta^{18}O$ relationships for the Laptev Sea and East Greenland Current[66,67], regions with relatively low $\delta^{18}O_{sw}$ linked to the Arctic Ocean or Arctic outflows respectively (the Laptev Sea is an Arctic shelf sea that receives large volumes of river run-off from Siberian rivers (22-34 PSU), while the East Greenland Current carries low salinity surface waters (32 PSU) out of the Arctic Ocean). It was assumed that these relationships remained the same down core.

Laptev Sea:	Salinity= ($\delta^{18}O_{sw}$ –18.86) = 0.5	R^2 = 0.98 ref-[66]
East Greenland:	Salinity= ($\delta^{18}O_{sw}$ –35.02) = 1.01	ref-[67]

The resulting curve, which is plotted as a 'smoothed curve-fit' in KaleidaGraph® with error envelopes representing limits determined by 2σ of the BWT brackets (Main Fig. 3C), provides coarse constraints on the evolution of Site 647 bottom water salinity in the late Eocene. As discussed above, its possible that the decreasing Mg/Ca between 37.5-35.5 Ma represents decreasing trace metal contamination rather than BW cooling. If this is the case then the BWTs around 37 Ma are too high, which would bias the salinities to too salty values. Thus, including or excluding the older Mg/Ca data does not change the conclusions. We have confidence in the Mg/Ca after 34 Ma and thus have δ^{18}Osw constrained there. The important point is that the subsurface densification signal is seen in the benthic foraminifera $\delta^{18}O$ record (increasing $\delta^{18}O$ from 37.5-35.5 Ma). It is impossible that this is an artifact of the Mg/Ca data.

Neodymium isotope methodology

Fish teeth and bone debris were hand-picked from the >63µm fraction of sieved sediment and cleaned to remove adhering debris. Initial experiments (see Supplementary information) indicated that a the 'simple cleaning method' of ref-[68] was sufficient. All samples were dissolved in 2M HCl, dried and converted to nitrate form prior to column chemistry. A standard two-stage ion chromatography procedure was used, which first isolated the REEs from the sample matrix using TRU Spec resin (100-120µm bead size) and then separated Nd from the other REE's with Ln-Spec resin (50-100µm bead size) (after ref-[69]). Neodymium isotope ratios were measured on a Nu Plasma MC-ICP-MS at Imperial College London in static mode. Instrumental mass bias was corrected for using a $^{146}Nd/^{144}Nd$ ratio of 0.7219. Samarium interference can be adequately corrected if the ^{144}Sm signal contributes less than 0.1% of the ^{144}Nd signal. The Sm contribution in all our samples was well below this level. Chemistry blanks were consistently below 10pg

Nd. Replicate analyses of the Nd standard JNdi yielded $^{143}Nd/^{144}Nd$ ratios from 0.512060 ± 0.000015 to 0.512251 ±0.000015 (n=116), dependent on daily running conditions over 12 months. The external reproducibility of our chemistry and mass spectrometry procedure was monitored using a fossil bone composite standard supplied by Clive Trueman (University of Southampton) yielding a $^{143}Nd/^{144}Nd$ ratio of 0.512377 ± 0.000028 (n=8 over 18 months), which agrees within error with previously published values[70,71]. We note that the standard material was digested for analysis following the methods in ref[70] for analytical consistency. Briefly, 50 mg of material was digested in 3M HNO_3 in a Teflon beaker at 130ºC. Any material remaining after this step was subjected to a further 48 hours digestion in a 3:1 mixture of 15M HNO_3 to 27M HF. To correct for the decay of ^{147}Sm to ^{143}Nd within the fish teeth over time we use rare earth element concentrations obtained in two samples from this site. Derived $^{147}Sm/^{143}Nd$ ratios of 0.129 and 0.134 are consistent with values reported in other studies[72-74]. We applied an average value of our measurements ($^{147}Sm/^{143}Nd$ = 0.132) to all remaining samples. All Nd isotope ratios are reported in epsilon notation (ε_{Nd}) (Supplementary Table 6). Comparative ε_{Nd} data in Figure 3 are listed in Supplementary Table S7.

Atlantic isotopic depth sections

We used standard techniques in ocean data assimilation to create homogenized and interpolated maps of isotopic values based on the sparse data (see Supplementary Table S1 for site information, data sources and a more complete set of maps; SI Figs 9A-L). For the transects the proxy data were placed on to a regular latitude-depth grid based on their reconstructed depths and palaeo-locations, and the natural neighbor regridding routines implemented in the NCAR Command Language were used to create interpolated, gridded values (https://www.ncl.ucar.edu/Document/Functions/Built-in/natgrid.shtml). Extrapolation beyond the convex hull of the kernel was not used. The background palaeogeography is based on Ref-[75] (hotspot reference frame). The differences in interpretation for our paper using the alternative Palaeomag reference frame described in the same study are negligible.

For the maps, the proxy records interpolated using the technique of Barnes-Cressman iterated objective analysis implemented in the NCAR Command Language (www.ncl.ucar.edu/Document/ Functions/Contributed/obj_anal_ic_Wrap.shtml). In this approach, each observation is assigned a circular radius of influence, R. Here, we used successive values of R of 9°, 8°, 6°, 4°, 2°, 1°. A first guess of the value at every grid point was made by including all observations within the region of influence of that grid point. A distance-weighted average of the differences between the first-guess fields and the actual observations was made, and this anomaly was added into the first-guess fields to calculate a second-guess field. Thus, observations from beyond the radius of influence were ignored in updating the field, and other observations closer to the initial observation were given greater weight. This was done for all grid points under consideration. The resulting fields were used as the basis for the next iteration, which was carried out with a smaller region of influence.

Data availability statement

The authors declare that lists of the sources of previously published data used in this study are available within the article and its Supplementary Information files. The new data are available at the Bolin Centre for Climate Research Database: http://bolin.su.se/data/Coxall-2018.

References

51 Schmitz, W. J. & McCartney, M. S. On the North Atlantic Circulation. *Rev. of Geophys.* **31**, 29-49 (1993).

52 Laughton, A. S. *et al.* Site 112, in *Initial Reports of the Deep Sea Drilling Project,* Vol. **12** (eds A.S. Laughton, W. A. Berggren *et al.*) 161-253 (US Goverment Printing Office, 1972).

53 Norris, R. D., Wilson, P. A., Blum, P. & the Expedition Scientists, *Proceedings of the Integrated Ocean Drilling Program*, **342**, doi:10.2204/iodp.proc.342.2014 (Integrated Ocean Drilling Program, 2014).

54 Miller, K. G. & Katz, M. E. in *Initial Reports of the Deep Sea Drilling Project,* Vol. **95** (eds C. W. Poag, A. B. Watts *et al.*) 267-298 (U.S. Goverment Printing Office, 1987).

55 Cande, S. C. & Kent, D. V. Revised calibration of the geomagnetic polarity timescale for the Late Cretaceous and Cenozoic. *J. Geophys. Res.* **100**, 6093-6095 (1995).

56 Zachos, J. C., Pagani, M., Sloan, L. C., Thomas, E. & Billups, K. Trends, rhythms, and aberrations in global climate 65 Ma to present. *Science* **292**, 686-693 (2001).

57 Zachos, J. C., Dickens, G. R. & Zeebe, R. E. An early Cenozoic perspective on greenhouse warming and carbon-cycle dynamics. *Nature* **451**, 279-283 (2008).

58 Lear, C. H. *et al.* Neogene ice volume and ocean temperatures: Insights from infaunal foraminiferal Mg/Ca paleothermometry. *Paleoceanography* **30**, 1437-1454 (2015).

59 Pearson, P. N. *et al.* Warm tropical sea surface temperatures in the Late Cretaceous and Eocene epochs. *Nature* **413**, 481-487 (2001).

60 Katz, M. E. *et al.* Early Cenozoic benthic foraminiferal isotopes: species reliability and interspecies correction factors. *Paleoceanography* **18**, 1024 (2003).

61 Rathburn, A. E., Corliss, B. H., Tappa, K. D. & Lohmann, K. C. Comparisons of the ecology and stable isotopic compositions of living (stained) benthic foraminifera from the Sulu and South China Seas. *Deep Sea Res. Pt 1. Oceanographic research papers* **43**, 1617-1646 (1996).

62 Boyle, E. A. Manganese carbonate overgrowths on foraminifera tests. *Geochim. Cosmochim. Acta* **47**, 1815-1819 (1983).

63 Boyle, E. A. & Keigwin, L. D. Comparison of Atlantic and Pacific paleochemical records for the last 215,000 years: changes in deep ocean circulation and chemical inventories. *Earth Planet. Sci. Lett.* **76**, 135-150 (1985).

64 Barker, S., Greaves, M. & Elderfield, H. A study of cleaning procedures used for foraminiferal Mg/Ca paleothermometry. *Geochem., Geophys., Geosystems* **4**, doi:10.1029/2003GC000559 (2003).

65 Marchitto, T. M. *et al.* Improved oxygen isotope temperature calibrations for cosmopolitan benthic foraminifera. *Geochim. Cosmochim. Acta* **130**, 1-11 (2014).

66 Mueller-Lupp, T., Erlenkueser, H. & Bauch, H. A. Seasonal and interannual variability of Siberian river discharge in the Laptev Sea inferred from stable isotopes in modern bivalves. *Boreas* **32**, 292-303 (2003).

67 Fairbanks, R. G., Charles, C. D. & Wright, J. D. in *Radiocarbon After Four Decades* (ed R. E. Taylor) 473-500 (Springer, 1992).

68 Martin, E. E. & Haley, B. A. Fossil fish teeth as proxies for seawater Sr and Nd isotopes. *Geochim. Cosmochim. Acta* **64**, 835-847 (2000).

69 Pin, C. & Zalduegui, J. S. Sequential separation of light rare-earth elements, thorium and uranium by miniaturized extraction chromatography: application to isotopic analyses of silicate rocks. *Analyt. Chimica Acta* **339**, 79-89 (1997).

70 Chavagnac, V. *et al.* Towards the development of a fossil bone geochemical standard: An inter-laboratory study. *Analyt. Chimica Acta* **599**, 177-190 (2007).

71 Scher, H. D. & Delaney, M. L. Breaking the glass ceiling for high resolution Nd isotope records in early Cenozoic paleoceanography. *Chem. Geol.* **269**, 329-338 (2010).

72 Thomas, D. J., Bralower, T. J. & Jones, C. E. Neodymium isotopic reconstruction of late Paleocene-early Eocene thermohaline circulation. *Earth Planet. Sci. Lett.* **209**, 309-322 (2003).

73 Martin, E. E. & Scher, H. A Nd isotopic study of southern sourced waters and Indonesian throughflow at intermediate depths in the Cenozoic Indian Ocean. *Geochem. Geophys. Geosystems* **7**, Q09N02 (2006).

74 Moiroud, M. *et al.* Evolution of the neodymium isotopic signature of neritic seawater on a northwestern Pacific margin: new constrains on possible end-members for the composition of deep-water masses in the Late Cretaceous ocean. *Chem. Geol.* **356**, 160-170 (2013).

75 Baatsen, M. *et al.* A generalised approach to reconstructing geographical boundary conditions for palaeoclimate modelling. *Clim. Past.* **12**, 4917-4942 (2016).

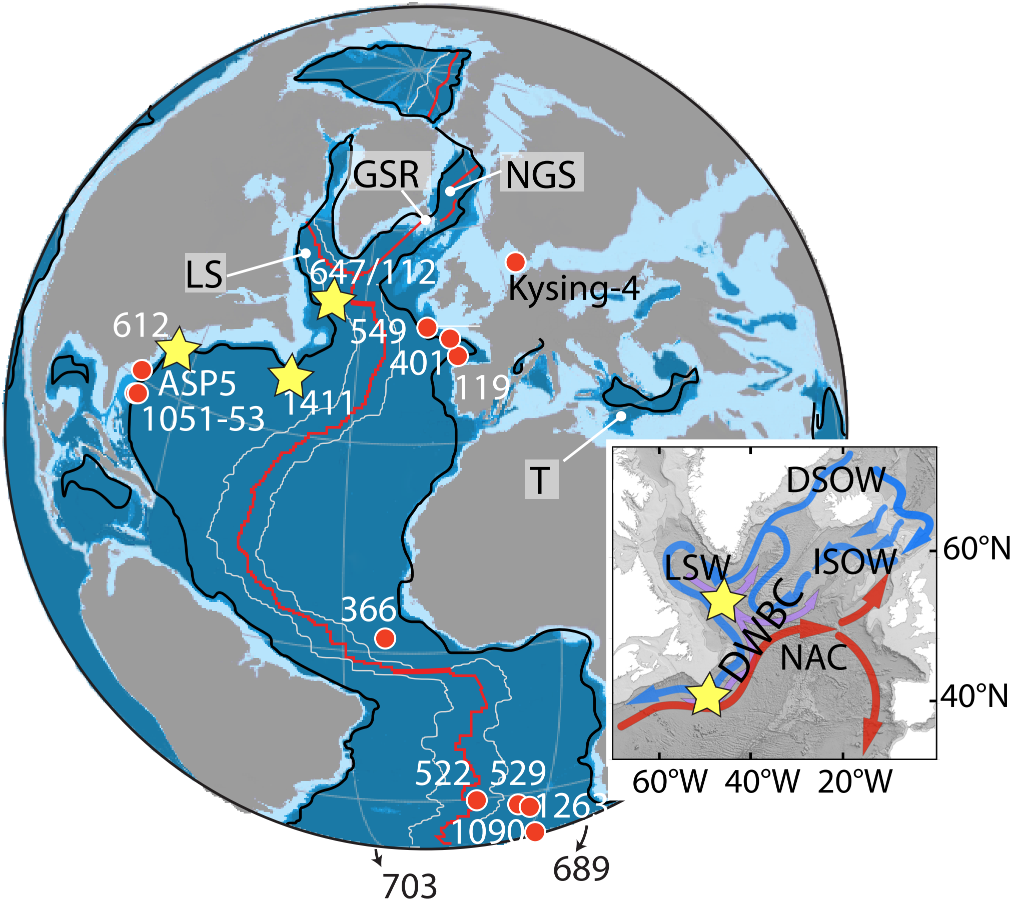
GSR
NGS
LS
647/112
Kysing-4
612
549
401
119
ASP5
1051-53
1411
T
DSOW
LSW
ISOW
DWBC
NAC
60°N
40°N
60°W
40°W
20°W
366
522
529
1263
1090
703
689

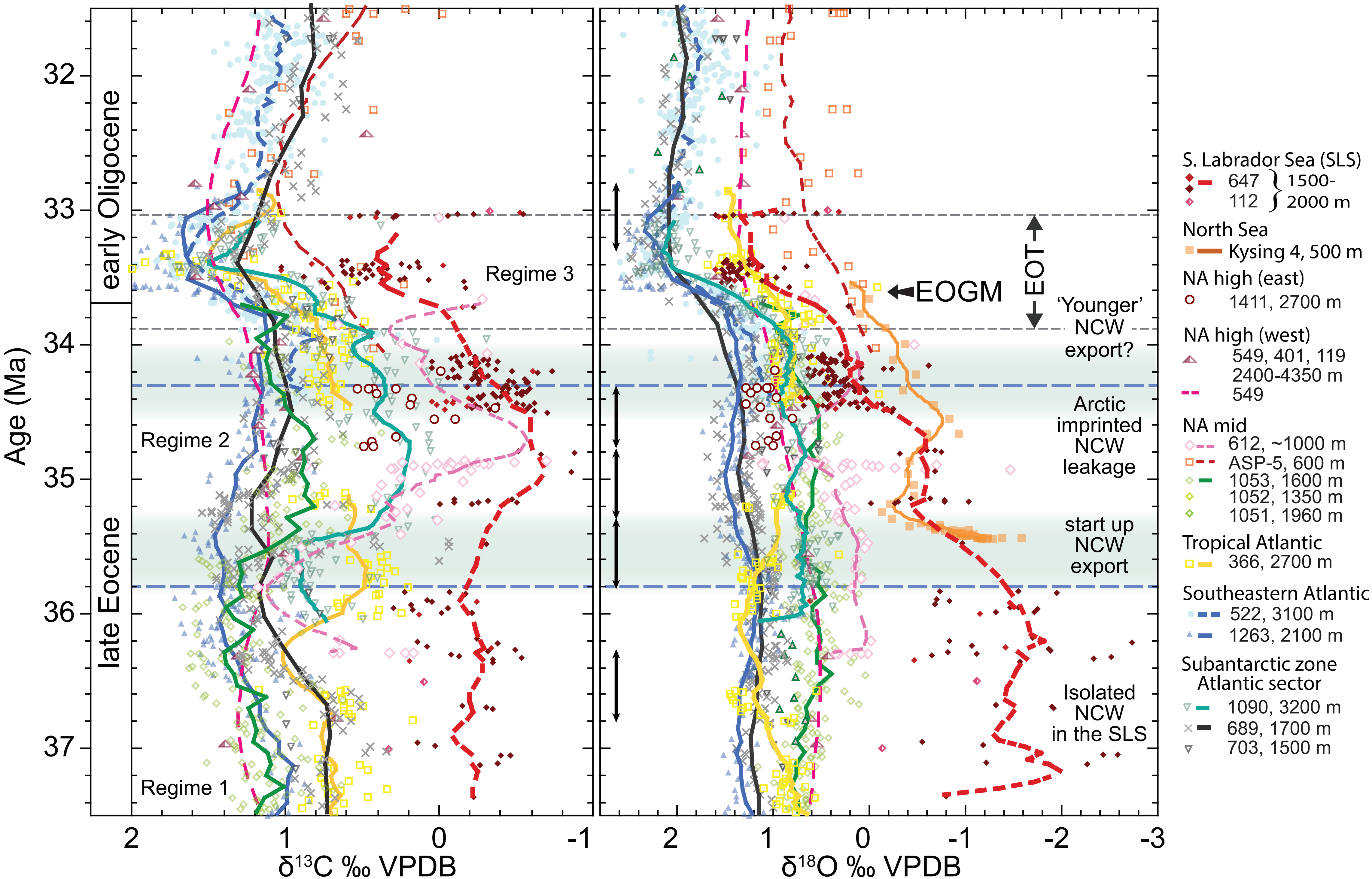

early Oligocene
late Eocene
Age (Ma)
32
33
34
35
36
37
Regime 3
Regime 2
Regime 1
δ13C ‰ VPDB
2
1
0
-1
δ18O ‰ VPDB
-2
-3
EOGM
EOT
'Younger' NCW export?
Arctic imprinted NCW leakage
start up NCW export
Isolated NCW in the SLS
S. Labrador Sea (SLS)
647
112
1500-2000 m
North Sea
Kysing 4, 500 m
NA high (east)
1411, 2700 m
NA high (west)
549, 401, 119
2400-4350 m
549
NA mid
612, ~1000 m
ASP-5, 600 m
1053, 1600 m
1052, 1350 m
1051, 1960 m
Tropical Atlantic
366, 2700 m
Southeastern Atlantic
522, 3100 m
1263, 2100 m
Subantarctic zone Atlantic sector
1090, 3200 m
689, 1700 m
703, 1500 m

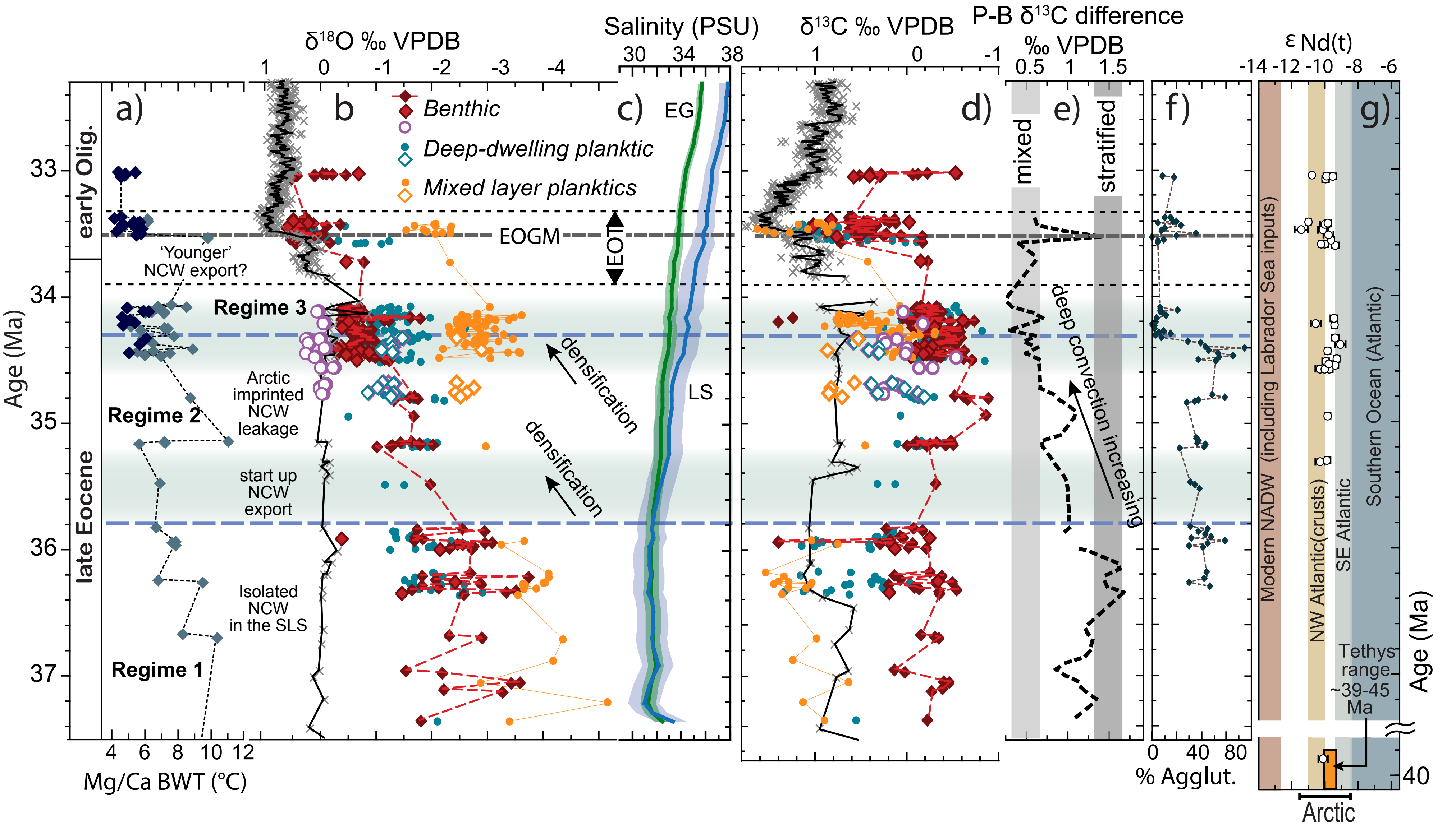

a)
b
c)
d)
e)
f)
g)
δ18O ‰ VPDB
Salinity (PSU)
δ13C ‰ VPDB
P-B δ13C difference
‰ VPDB
ε Nd(t)
Age (Ma)
Mg/Ca BWT (°C)
% Agglut.
Benthic
Deep-dwelling planktic
Mixed layer planktics
early Olig.
late Eocene
EOGM
EOT
EG
LS
'Younger'
NCW export?
Regime 3
Regime 2
Regime 1
Arctic
imprinted
NCW
leakage
start up
NCW
export
Isolated
NCW
in the SLS
densification
densification
mixed
stratified
deep convection increasing
Modern NADW (including Labrador Sea inputs)
NW Atlantic(crusts)
SE Atlantic
Southern Ocean (Atlantic)
Tethys
range
~39-45
Ma
Arctic

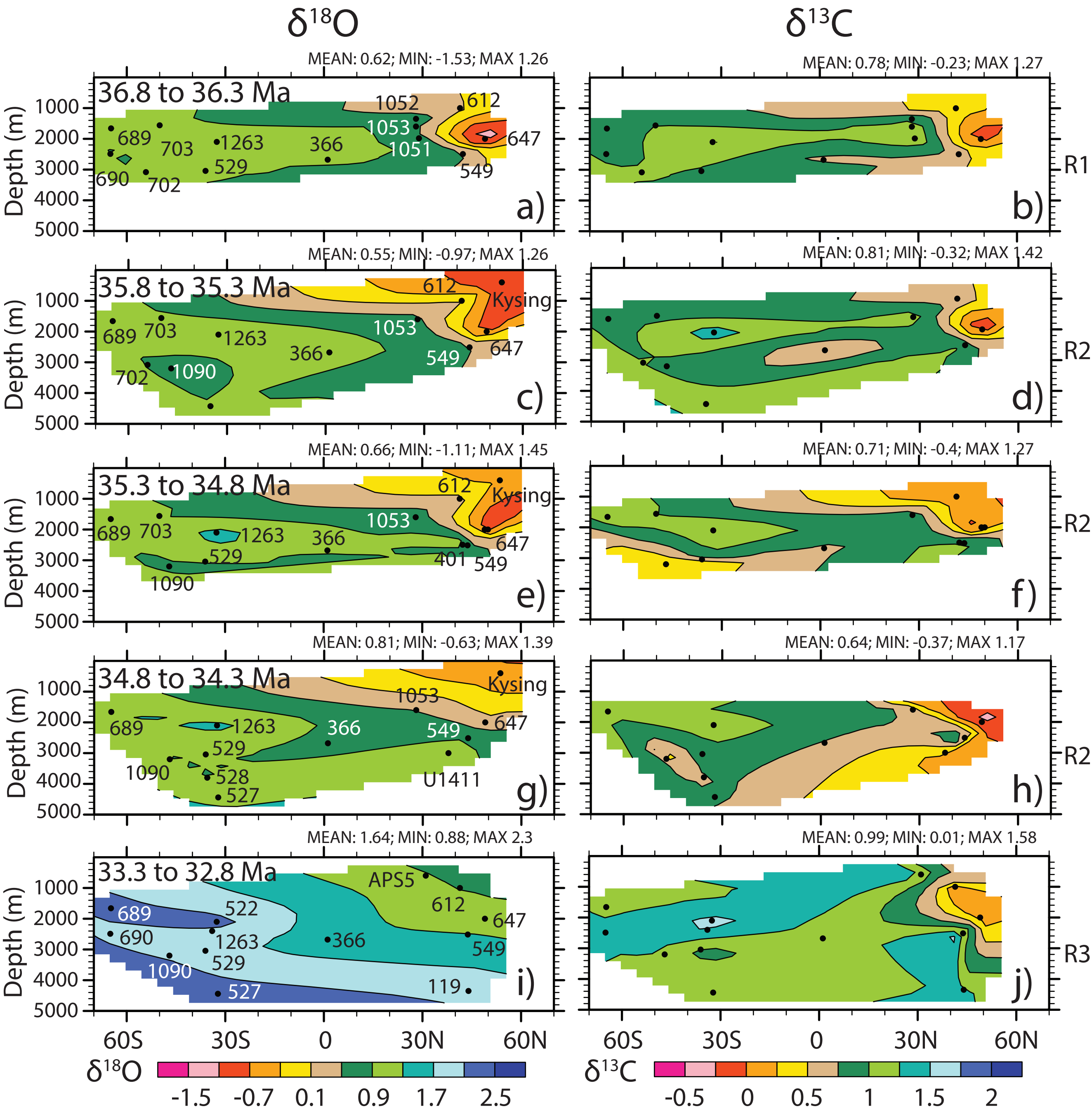

δ18O
δ13C
MEAN: 0.62; MIN: -1.53; MAX 1.26
36.8 to 36.3 Ma
1052
612
1053
647
689
703
1263
366
1051
690
702
529
549
a)
MEAN: 0.78; MIN: -0.23; MAX 1.27
b)
R1
MEAN: 0.55; MIN: -0.97; MAX 1.26
35.8 to 35.3 Ma
612
Kysing
1053
689
703
1263
366
647
549
702
1090
c)
MEAN: 0.81; MIN: -0.32; MAX 1.42
d)
R2
MEAN: 0.66; MIN: -1.11; MAX 1.45
35.3 to 34.8 Ma
612
Kysing
1053
689
703
1263
366
647
529
401
549
1090
e)
MEAN: 0.71; MIN: -0.4; MAX 1.27
f)
R2
MEAN: 0.81; MIN: -0.63; MAX 1.39
34.8 to 34.3 Ma
Kysing
1053
689
1263
366
549
647
529
1090
528
527
U1411
g)
MEAN: 0.64; MIN: -0.37; MAX 1.17
h)
R2
MEAN: 1.64; MIN: 0.88; MAX 2.3
33.3 to 32.8 Ma
APS5
612
689
522
647
690
1263
366
549
529
1090
527
119
i)
MEAN: 0.99; MIN: 0.01; MAX 1.58
j)
R3
Depth (m)
1000
2000
3000
4000
5000
60S
30S
0
30N
60N
δ18O
-1.5
-0.7
0.1
0.9
1.7
2.5
δ13C
-0.5
0
0.5
1
1.5
2